Seismic Fragility Analysis of Turbine Building in Nuclear Power Plant Based on the Open-source Software OpenSees

Qiang Pei, Jiaxing Di, Yingzhu Zhong, Hongshuai Liu, Pengfei Qi, Di Cui, and Xinqi Weng

***Abstract*—Due to the uneven distribution of quality and stiffness in the turbine building of a Nuclear Power Plant (NPP), as well as the indirect influence of concrete strength and column reinforcement ratio on the Seismic Fragility Analysis (SFA) results, the SFA of the turbine building under beyond the design basis earthquake has not been fully studied. This article studies the influence of actual seismic waves on the damage of turbine buildings and evaluates the seismic behavior of structures through Incremental Dynamic Analysis (IDA). The failure probability of turbine buildings under different Peak Ground Acceleration (PGA) is calculated, and the influence of concrete strength and column reinforcement ratio on the seismic fragility curve of turbine buildings is studied. The research results indicate that the turbine building designed and verified in this article can effectively control the risk of earthquake collapse and has a certain degree of safety redundancy. When the column reinforcement ratio is between 1.1% and 1.8%, the lower the reinforcement ratio, the higher the failure probability of structures. Compared to C30 and C40, the structure using C50 concrete has the lowest failure probability.**

Manuscript received September 23, 2024; revised January 10, 2025. This research was supported by Dalian University Research Platform Project (202301ZD01), the National Natural Science Foundation of China (grant no. 51878108), Key Laboratory for Prediction & Control on Complicated Structure System of the Education Department of Liaoning Province(grant no. DLSZD2023011), Science and Technology Innovation Foundation of dalian (grant no. 2023JJ12GX012), Students' Training Program of Innovation and Entrepreneurship of Dalian University (grant no. D202404011305477487) and the Department of Science and Technology Guidance Plan Foundation of Liaoning Province (grant no. 2019JH8/10100091).

Qiang Pei is a professor of the Key Laboratory for Prediction & Control on Complicated Structure System of the Education Department of Liaoning Province, Dalian University, Dalian 116622, China (email: pqiem@163.com).

Jiaxing Di is a postgraduate student of College of Civil Engineering and Architecture, Dalian University, Dalian 116622, China (email: 13052670250@163.com).

Yingzhu Zhong is a postgraduate student of College of Civil Engineering and Architecture, Dalian University, Dalian 116622, China (email: zyzhu0229@163.com).

Hongshuai Liu is a professor of College of Civil Engineering and Architecture, Hebei University, Baoding 071002, China (email: 13050960250@163.com).

Pengfei Qi is a PhD candidate of Institute of Geophysics, China Earthquake Administration, Beijing 100081, China (email: q291990@163.com).

Di Cui is an associate professor of School of Civil Engineering, Dalian Jiaotong University, Dalian 116028, China (Corresponding author, phone: 86-13898690826; email: cuidip@163.com).

Xinqi Weng is an undergraduate of College of Civil Engineering and Architecture, Dalian University, Dalian 116622, China (email: 15604178593@163.com).

***Index Terms*—Nuclear power plant (NPP), Turbine building, Seismic fragility analysis (SFA), Incremental dynamic analysis (IDA), Seismic behavior**

I. Introduction

The Fukushima leakage incident in March 2011 in Japan[1,2] indicates that we need to improve structural defense capabilities against extreme external events to ensure that small probability but serious consequences beyond-design basis accidents are properly considered in site selection and design[3] and to maintain appropriate safety margins[4]. Further reducing the seismic risk of NPPs and enabling them to continue safe operation after beyond design basis accidents have become a common goal in the global engineering community[5]. Therefore, it is of great practical significance to evaluate the seismic behavior of NPPs under beyond-design basis earthquake action[6].

Seismic Probability Risk Assessment (SPRA) is an effective method for evaluating the safety and regulatory requirements of NPP construction and operation[7,8]. The basic requirement of SPRA is to conduct SFA on the structure, and establish the relationship between seismic representative attributes and the failure probability of components, structures[9], systems, or equipment[10] through extensive numerical simulations[11,12]. IDA is a parameter method developed based on traditional elastic-plastic dynamic time history analysis to study SFA[13], and it has been used by the Federal Emergency Management Agency (FEMA) as the main analysis method for evaluating the seismic behavior of the entire structure in case of collapse and widely applied in the field engineering seismic resistance[14,15]. Feng Cheng et al.[16] conducted a fragility analysis of the NPP structure under real and spectrum-compatible seismic waves, and provided the fragility assessment and maximum tension strain contours of the AP1000 NPP. Chunfeng Zhao et al.[17] presents a fragility assessment to evaluate the effects of far-field earthquakes on the damage of the AP1000 nuclear shielding buildings, by using IDA and Multiple Stripes Analysis methods. Fernanda de Borbón et al.[18] presents a numerical study of the influence of various parameters on the seismic response of the CAREM-25 NPP located in Argentina. Duy-Duan Nguyen et al.[19] investigate the efficiency of various structural modeling schemes for evaluating seismic performances and fragility of the reactor containment building structure in the advanced power reactor 1400 NPP. Chanyoung Kim et al.[20] investigate the effects of earthquake characteristics on the seismic fragility of concrete containments housing the OPR-1000 reactor.

It can be seen that due to the demand for performance-based seismic design, increasingly researchers have adopted the IDA method to evaluate the demand capacity of shielding buildings, auxiliary buildings, and pipeline facilities in NPP under earthquake action, and have achieved fruitful results[21]. It should be emphasized that the turbine building is arranged adjacent to the shielding building, and the collapse of the turbine building may endanger the safety of the shielding building, so the seismic behavior of the turbine building must consider its impact on the shielding building[22]. For non-safety level structures that may endanger the functions of Class I seismic buildings, it is necessary to ensure that they do not collapse under extremely safe seismic motion[23,24]. However, due to the uneven distribution of quality and stiffness, complex types of internal equipment, multiple staggered floors, and large areas of floor openings in the turbine building, the seismic design and risk assessment of the structure is more remarkably complex[25], and the impact of actual seismic waves on the SFA of the structure has not been fully studied.

The turbine building adopts a frame-bent structure. The seismic response characteristics and damage of frame-bent structures are more complex than those of frame structures and bent frame structures[26], exhibiting more significant spatial effects, and its seismic design has special requirements[27,28]. Moreover, the bearing capacity of the frame structure is mainly manifested through the mechanical properties of the beams and columns, so the concrete strength and column reinforcement ratio will indirectly affect the SFA of the frame-bent structure[29,30]. The concrete strength and column reinforcement ratio need to be given special consideration when conducting the SFA of turbine buildings.

As mentioned before, it is necessary to conduct an SFA study of turbine buildings in NPP based on the IDA method as soon as possible, considering the factors of concrete strength and column reinforcement ratio.

In order to evaluate the safety and reliability of the turbine building under earthquake action, study its seismic response, and explore its fragility under different intensities of seismic motion, this paper first structurally designs and verifies turbine building based on actual engineering cases, as well as establishes and verifies finite element model of the structure. Then, based on the theory of Earthquake Probability Risk Assessment, the IDA method was used to study the seismic response of the turbine building, calculate the failure probability, and draw the fragility curve of the structure under different seismic intensity parameters. Finally, parameter analysis of concrete strength and column reinforcement ratio under nine cases was conducted to explore their impact on the SFA of turbine buildings.

II. Finite element model

A. Engineering overview and PKPM modeling

The main building of a conventional island in NPP consists of a turbine building, a deaeration room, and internal nuclear power equipment. According to the “Code for Seismic Design of Building Structures”(GB 50011-2010) and “Code for Design of Concrete Structures”(GB 50010-2010), the turbine building with frame-bent structure was designed. The layout plan of the planar column network and the section diagram of the third axis are shown in Fig. 1 and Fig. 2, respectively. Using PKPM for the structural design of the turbine building, the span of the A-B axis is 44m, and the span of the B-C axis is 15m.

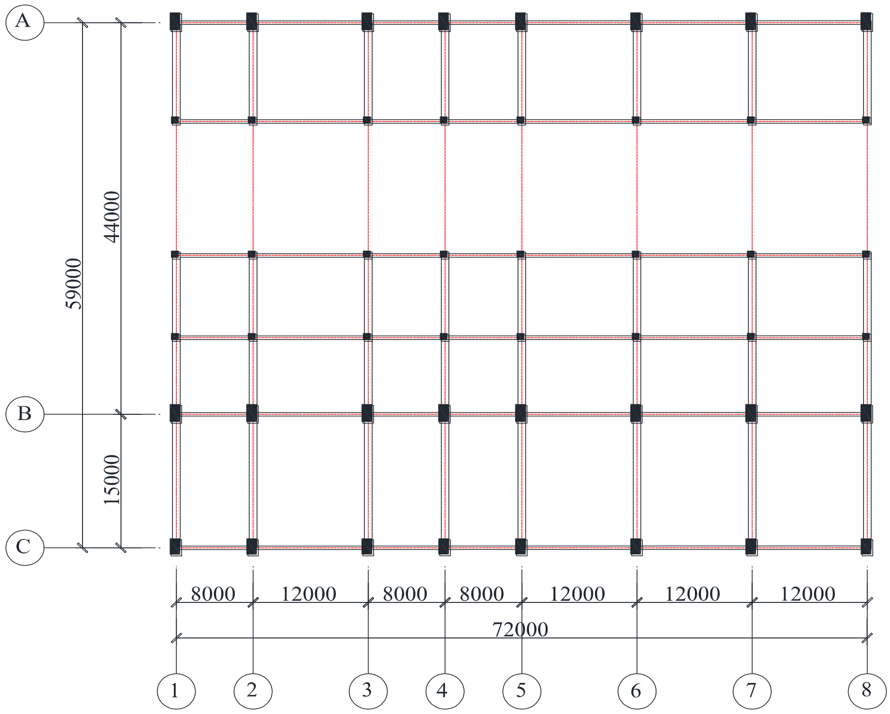

Fig. 1. Layout plan of the planar column network

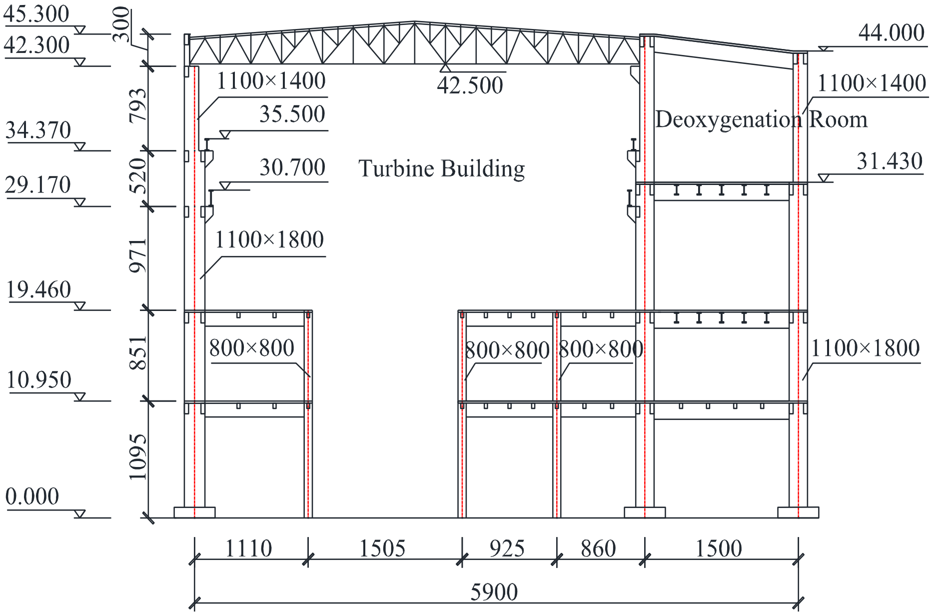

Fig. 2. Section diagram of the third axis

The fortification earthquake group is group 3, the building site category is class II, the seismic fortification intensity is 8 degrees, the design basic acceleration is 0.1g, and the model concrete grade is C40. The column reinforcement diagram of the turbine building is shown in Fig. 3. The minimum reinforcement ratio of the structural checking and the minimum reinforcement ratio of the longitudinally stressed steel bars on one side are both equal or lesser than 5%, and the middle moment of the longitudinally stressed reinforcements perpendicular to the bending moment plane in the bent column is 230mm (the specification is less than 350mm).

Load conditions: (1) Constant load, mainly for the structure weight, calculated automatically by the software; (2) Crane load: the crane selected in this project is A5, 20/5t, calculated: $D_{\max}$ value of 631.80kN, $D_{\min}$ value of 210.20kN, $T_{\max}$ value of 20.60kN; (3) Seismic action, considering the torsion effect under bidirectional seismic action; (4) Wind load is 0.55kN/m^2, snow load is 0.40 kN/m^2; (5) The floor live load is 2.00kN/m^2, and the roof live load is 2.00kN/m^2.

B. Finite element modeling

The finite element modeling of turbine building is carried out by OpenSees software[31]. Due to the irregular arrangement of structural space and the complexity of dynamic analysis, and the main focus of this article on analyzing overall collapse, it is necessary to simplify the analysis model reasonably. Among them, the beam-column connection adopts a rigid connection, and the steel roof truss between the A-axis and B-axis is replaced by an infinitely rigid rod. At the same time, the bottom column connected to the foundation is defined according to the fixed connection method.

OpenSees provides a wide range of section types. Fiber elements not only need to simulate accurately and converge simply but also need to be able to simulate the actual seismic response of the structure. This study chose fiber units based on the flexibility method (Nonlinear Beamcolumn). Concrete is simulated using Concrete01 material, the skeleton curve characteristic parameters of the constrained zone concrete are calculated using the Mander model, and the reinforcements are simulated using Steel02 material. The nonlinear beam-column fiber element satisfies the following basic assumptions[32]: (1) the fiber section satisfies the assumption of a flat section; (2) The beam-column element is divided into several integral segments, and the constitutive relationship of each fiber within each segment remains consistent (as shown in Fig. 4); (3) Neglecting the effects of bond-slip and shear deformation.

This article uses the number of cross-sectional divisions of reinforced concrete components these articles [12,33] as a reference for dividing the fiber elements. Fig.5 shows the division based on the fiber model of beam-column elements. Taking column A as an example, the column elements are divided into fiber sections of the concrete core area, fiber sections of the concrete protective layer, and fiber sections of reinforcement.

The structure adopts Rayleigh damping in OpenSees[34], which means that the size of the damping matrix is related to the mass matrix and stiffness matrix of the structure. The relationship between damping, stiffness, and mass is determined according to the literature[35]. The schematic diagram of the final established OpenSees finite element model is shown in Fig. 6.

C. Finite element model checking

The comparison of the first three natural vibration periods of the model established using PKPM and Opensees software is shown in Table I. The results show that the first three natural vibration periods of PKPM and OpenSees are relatively similar, with an error of no more than 3%, indicating that the two models have good similarity.

To ensure the accuracy of the finite element model, the turbine building data obtained from engineering measurements were compared with the modal analysis results of OpenSees (Table II). The error between the finite element model and the experimental modal analysis does not exceed 3%, indicating that the finite element model established using OpenSees has an engineering reference value.

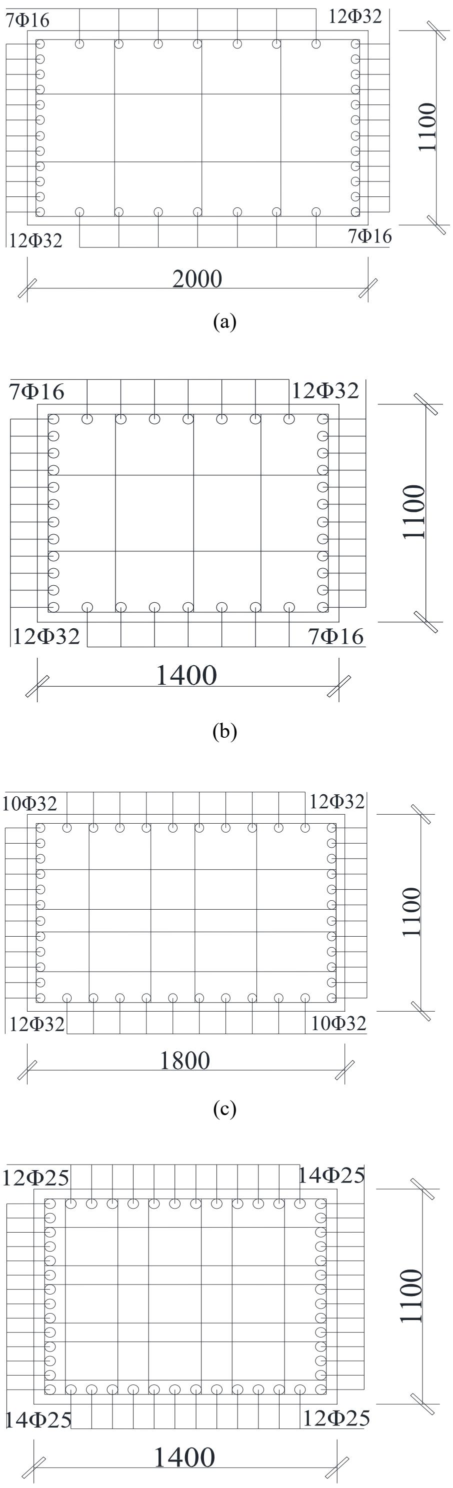

Fig. 3. Column reinforcement diagram of turbine building: (a) The 0-34.37m interval reinforcement diagram of A-axis and B-axis columns, (b) The 31.43-42.30m interval reinforcement diagram of A-axis and B-axis columns, (c) The 0-34.37m interval reinforcement diagram of C-axis columns, (d) The 31.43-42.30m interval reinforcement diagram of C-axis columns

TABLE I
COMPARISON OF THE FIRST THREE PERIODS OF THE STRUCTURE

Period / s	T_{OS}	T_{PK}	Error / %
T_1	1.653	1.605	- 2.90
T_2	1.615	1.628	+ 0.80
T_3	1.515	1.542	+ 1.78

TABLE II
COMPARISON OF STRUCTURE CYCLE CALCULATION

Period / s	OpenSees	Site measurement	Error / %
Vibration mode 1	0.426	0.417	- 2.11
Vibration mode 2	0.118	0.121	+ 2.54
Vibration mode 3	0.063	0.062	- 1.59

III. FRAGILITY ANALYSIS

Seismic fragility is the probability of characterizing a specific safety threshold[36]. There are five methods to characterize fragility. The damage fragility used in this paper is the probability that the Damage Measure (DM) of seismic response exceeds a specific safety threshold that characterizes the seismic load Intensity Measure (IM)[37]. The DM is derived from the quantitative Engineering Demand Parameters (EDP) that can be expressed by the project[38,39]. The seismic response DM of the structure and the ground motion intensity index IM need to meet the following conditions[40]:

$$\mathrm{DM} = \alpha\,(\mathrm{IM})^{\beta} \tag{1}$$

Take logarithm on both sides of the above formula:

$$\ln(\mathrm{DM}) = \ln(\alpha) + \beta \cdot \ln(\mathrm{IM}) = a + b \cdot \ln(\mathrm{IM}) \tag{2}$$

Where $a = \ln(\alpha)$ is the intercept of the function, $b = \beta$ is the slope of the function, and both are constants. The ground motion intensity parameter PGA and the structural damage index $\theta_{\max}$ are brought into the model formula:

$$\ln(\theta_{\max}) = a + b \cdot \ln(\mathrm{PGA}) \tag{3}$$

The linear function can be obtained by data fitting so that the specific values of parameters α and β can be obtained. The fragility curve of the structure in the seismic fragility calculation is expressed as follows:

$$P_{DV\,|\,IM}(0\,|\,\mathrm{PGA}) = \sum P_{DV\,|\,LS}(0\,|\,C)\, P_{DM\,|\,IM}(Z > C\,|\,\mathrm{PGA}) \tag{4}$$

In the formula: P represents the probability of structural damage exceeding a certain state point; IM represents the ground motion intensity index (the ground motion intensity in this paper is PGA); DM represents the damage index of the structure; DV represents decision variables; LS denotes the limit state. According to the Eq. (4), the failure probability of the specific stage of the structure is:

$$\mathrm{P}_f = \Phi\left(\frac{\ln\left[\alpha\,(\mathrm{PGA})^2 \,/\, \hat{\mathrm{C}}\right]}{\sqrt{\beta_c^2 + \beta_d^2}}\right) \tag{5}$$

In the formula: P_f represents the probability that the response of the structure under seismic action exceeds a certain state; $\hat{\mathrm{C}}$ represents the median of structural capacity, which is taken as the limit value of each limit state, 0.0025 in Immediate Occupancy state, 0.004 in Life Safety state, 0.01 in Collapse Prevention state and 0.025 in Incipient Collapse state. $\sqrt{\beta_c^2 + \beta_d^2}$ can be obtained by statistics. When the fragility curve takes PGA as the independent variable, $\sqrt{\beta_c^2 + \beta_d^2}$ takes 0.5 uniformly.

A. Determination of ground motion intensity index and structural damage index

The selection of ground motion intensity index IM is one of the challenges in SFA[41]. The ground motion intensity index generally requires adjustable, monotonically increasing, and proportional to the amplitude modulation coefficient[42]. At present, the commonly used IM for the IDA method are: the peak ground acceleration (PGA), the peak ground velocity (PGV), the peak ground displacement (PGD), the acceleration spectrum Sa (T_1, 5%) corresponding to the basic period of the structure with a damping ratio of 5%, etc. Due to the difference of different ground motion intensity indexes, the PGA or the Sa (T_1, 5%) is usually used as the ground motion intensity index IM of earthquakes in the seismic design practice and seismic response analysis of NPP[43]. In this paper, the PGA is selected as the ground motion intensity index IM.

The seismic response index DM of the structure is a variable that reflects the change of the structure with the increase of the ground motion amplitude modulation coefficient[44]. The commonly used DM indicators are: maximum base shear, maximum floor ductility, maximum vertex displacement angle θ_{roof}, maximum interlayer displacement angle $\theta_{\max}$, etc[45]. Because the selection of DM is mainly related to the analysis purpose and structural characteristics, the maximum inter-story displacement angle $\theta_{\max}$ is generally used as DM. The maximum inter-story displacement angle is directly related to the degree of structural damage, structural collapse resistance, and joint rotation, which can better reflect the seismic performance of the structure. The relative strength relationship between beam and column, axial compression ratio, concrete strength grade, stirrup ratio, shear span ratio, and reinforcement ratio can affect the displacement angle between layers of the structure. The maximum inter-story displacement angle can reflect the inter-story displacement ductility and overall displacement ductility of the structure, and the performance of the structure can be fully understood by analyzing it. Therefore, this paper determines to select the maximum interlayer displacement angle $\theta_{\max}$ as the structural damage index[30].

B. Selection and amplitude modulation of seismic wave

When different ground motions are input, the difference in the displacement and internal force results of the structural system obtained by the bottom shear method or the mode decomposition response spectrum method can sometimes reach several times or even dozens of times[28]. Therefore, in the analysis of structural seismic fragility, it is particularly important to reasonably select ground motion[46]. There are many ground motion selection methods, among which the selection method based on conditional spectrum and generalized conditional strength parameters are the research hotspots in recent years[47,48]. ATC-63 aims to achieve wide applicability and has developed a set of criteria for selecting earthquake motion records based on station and seismic information[49]. In order to reduce the influence of near-field effects[50], a far-field motion selection set containing 22 far-field motion records is provided. According to the eight wave selection principles proposed in ATC-36, 22 natural waves that meet the conditions are selected from the PEER Strong Motion Database NGA-West2 of the University of California, Berkeley. The selected model in this article is located in a Class II site, similar to the Class D site in NEHRP. The seismic records of the Class D site in the ATC-63 far-field seismic selection set are selected as the input seismic motion for this article. The Seismic wave record information is shown in Table III.

In this paper, the equal-step method of increasing 0.1g each time is used to determine the amplitude modulation coefficient to modulate the seismic wave. The amplitude modulation rule is shown in Eq. (6):

$$A'(\mathrm{t}) = \frac{\alpha'_{\max}}{\alpha_{\max}} A(\mathrm{t}) \tag{6}$$

In the formula: $\alpha'_{\max}$ represents the maximum acceleration of time history analysis (0.07g, 0.2g, 0.4g); $\alpha_{\max}$ represents the maximum peak acceleration of the selected ground motion; A(t) represents the variation of natural ground motion with time; A'(t) represents the variation of natural ground motion with time after amplitude modulation.

C. Division of performance levels

In order to effectively describe the damage to the turbine building structure's underground motion, it is necessary to define the corresponding performance level (damage limit state). In this paper, referring to the introduction of FEMA 356 and SEACO Vision 2000, the different performance levels of the structure at the four limit state points of IO, LS, CP, and IC are divided by using the limit value of the inter-story displacement angle of the bent plant proposed in Reference, as shown in the Table IV.

D. IDA analysis of structure

1) Single IDA curve

Firstly, the amplitude of the Superstition Hills seismic wave is adjusted. The maximum inter-story displacement angle $\theta_{\max}$ is used as the X-axis, and the peak acceleration is used as the Y-axis. The three-spline interpolation method[51] is used to connect the points to obtain the entire IDA curve. The curve of the maximum interlayer displacement angle $\theta_{\max}$ and the maximum peak acceleration (PGA) is shown in Fig. 7.

TABLE IV
LIMITS OF INTERLAYER DISPLACEMENT ANGLE AT DIFFERENT PERFORMANCE LEVELS

Structural performance level	Limits of interlayer displacement Angle
Immediate Occupancy (IO)	0.25%
Life Safety (LS)	0.40%
Collapse Prevention (CP)	1.00%
Incipient Collapse (IC)	2.50%

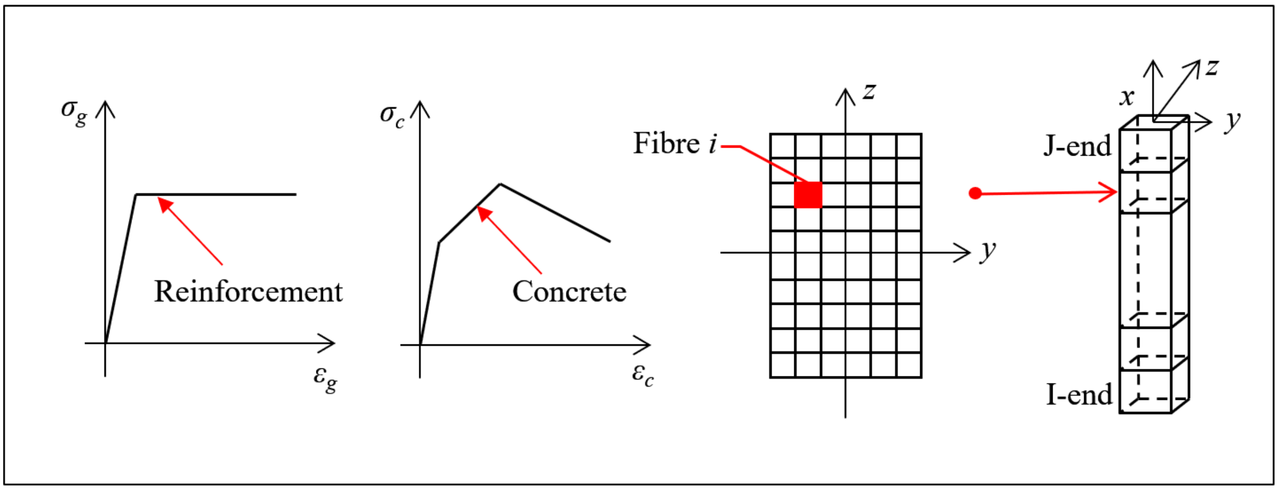

Fig. 4. Reinforced concrete constitutive model and beam column element division

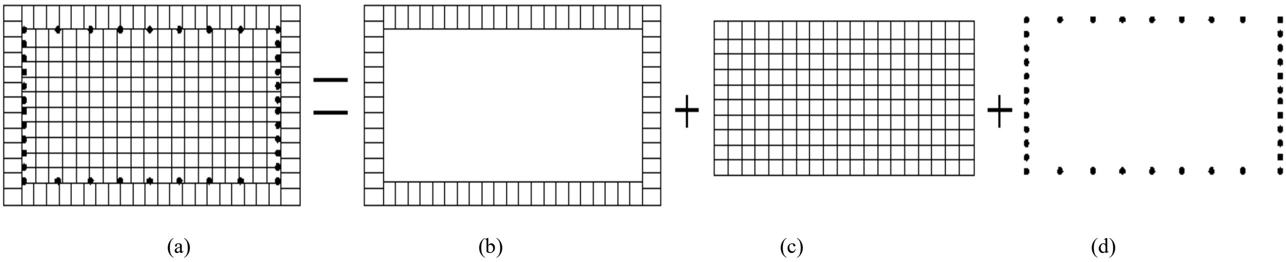

Fig. 5. Fiber sections: (a) Division of fiber cross-section in components, (b) Fiber of the concrete protective layer, (c) Fiber of the concrete core area, (d) Fiber of the reinforcement

TABLE III
SEISMIC WAVE RECORD INFORMATION

ID	Earthquake name	Time	Magnitude	Interval / s	Duration / s	Analysis steps	PGA / g	Magnitude
1	Northridge, USA	1994	6.7	0.0100	29.98	2998	0.52	6.7
2	Northridge, USA	1994	6.7	0.0100	19.98	1998	0.48	6.7
3	Duzce, Turkey	1999	7.1	0.0100	55.89	5589	0.82	7.1
4	Hector mine, USA	1999	7.1	0.0100	45.30	4530	0.34	7.1
5	Imperial valley, USA	1979	6.5	0.0100	99.91	9991	0.35	6.5
6	Imperial valley, USA	1979	6.5	0.0050	39.03	3903	0.38	6.5
7	Kobe, Japan	1995	6.9	0.0100	40.95	4095	0.51	6.9
8	Kobe, Japan	1995	6.9	0.0100	40.95	4095	0.24	6.9
9	Kocaeli, Turkey	1999	7.5	0.0050	27.18	2718	0.36	7.5
10	Kocaeli, Turkey	1999	7.5	0.0050	29.99	2999	0.22	7.5
11	Landers, USA	1992	7.3	0.0200	43.98	4398	0.24	7.3
12	Landers, USA	1992	7.3	0.0039	28.00	2800	0.42	7.3
13	Loma Prieta, USA	1989	6.9	0.0050	39.95	3995	0.53	6.9
14	Loma Prieta, USA	1989	6.9	0.0050	39.94	3994	0.56	6.9
15	Manjil, Iran	1990	7.4	0.0200	53.52	5352	0.51	7.4
16	Superstition, USA	1987	6.5	0.0050	39.99	3999	0.36	6.5
17	Superstition, USA	1987	6.5	0.0100	22.29	2229	0.45	6.5
18	Mendocino, USA	1992	7.0	0.0200	35.98	3598	0.55	7.0
19	Chichi, China	1999	7.6	0.0050	89.99	8999	0.44	7.6
20	Chichi, China	1999	7.6	0.0050	90.00	9000	0.51	7.6
21	San Fernando, USA	1971	6.6	0.0100	27.99	2799	0.21	6.6
22	Friuli, Italy	1976	6.5	0.0050	36.34	3634	0.35	6.5

The results show that when $\theta_{max} = 0.0025$, PGA = 0.35g reaches the Immediate Occupancy (IO) limit state; when $\theta_{max} = 0.004$, PGA = 0.46g reaches the Life Safety (LS) limit state; when $\theta_{max} = 0.01$, PGA = 0.83g reaches the Collapse Prevention (CP) limit state; when $\theta_{max} = 0.025$, PGA = 1.42g, the Incipient Collapse (IC) limit state is reached.

2) IDA curve cluster

Using the same analysis method, the PGA of 22 seismic waves was adjusted, and the PGA increment after amplitude adjustment was 0.1g. When the maximum inter-story displacement angle is greater than 0.1% or the slope of the IDA curve is less than 20% of the initial slope, the structure is considered to collapse and stop the analysis. Using the same method to draw the IDA curve, the final IDA data is shown in Fig. 8.

Since the shape of the IDA curve is related to the selected seismic record, the response of the structure to different seismic waves will be discrete, so it is necessary to process the discrete data by the quantile regression method in the nonparametric method. The IDA curves obtained by analysis and processing are summarized into 16%, 50%, and 84% quantile curves, and these three quantile curves are used to characterize the average level and discrete type of IDA curve clusters. The limit state points of the IDA percentile curve are shown in Table V. In order to improve the calculation accuracy, this paper intercepts the maximum interlayer displacement angle with θ_{max} of 0-0.04, as shown in Fig. 9.

E. Fragility analysis results

1) Seismic probabilistic demand model

According to the fragility theory and related calculation methods, the regression analysis of the data obtained from the IDA is carried out. The logarithm of PGA is used as the independent variable[52], and the logarithm of θ_{max} is used as the dependent variable to establish the linear function ln (θ_{max}) = a + b · ln (PGA) regression analysis diagram is shown in Fig. 10. Through the linear regression diagram and regression curve, a = - 4.20646, b = 0.99101 can be obtained. Bring a and b into Eq. (3), and the demand probabilistic function of turbine building is:

$$\ln(\theta_{max}) = -4.20646 + 0.99101 \ln(\mathrm{PGA}) \quad (7)$$

Attainable $\alpha = e^a = 0.014899$, $\beta = b = 0.99101$.

2) Seismic fragility curve

The fragility curve is a key tool for seismic probabilistic safety assessment at the NPP level[47]. The fragility curve can be obtained by simulating the structural response with the damage data observed after the earthquake[53]. The mechanical solution method of the fragility curve is to bring the obtained α and β into Eq. (5) to obtain the turbine building exceeding probability curve of Eq. (7). The PGA is brought into the turbine building exceedance probability curve, and the fragility curve is drawn as shown in Fig. 11.

$$P_f = \Phi\left(\frac{\ln[0.014899\,(\mathrm{PGA})^{0.99101} / \hat{C}]}{\sqrt{\beta_c^2 + \beta_d^2}}\right) \quad (7)$$

It can be clearly seen from the fragility curve that the whole response process of the turbine building from linear elasticity to elastoplasticity to overall collapse under different intensity levels of earthquakes. Under the action of seismic waves, the structure is easy to achieve Immediate Occupancy, and it is not easy to Incipient Collapse. When PGA = 0.4 g, the exceedance probability of Immediate Occupancy (IO) is 96.1%, the exceedance probability of Life Safety (LS) is 79.2%, the exceedance probability of Collapse Prevention (CP) is 15.4%, and the exceedance probability of Incipient Collapse (IC) is 0.2%. It can ensure that the structure does not collapse under the condition of rare earthquakes in the 8-degree area (the probability of exceeding the limit state in the 8-degree area is shown in Table VI, and has a certain safety reserve.

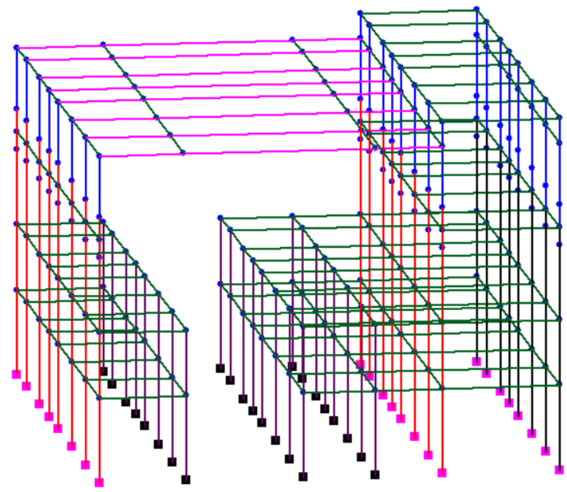

Fig. 6. OpenSees finite element model of turbine building

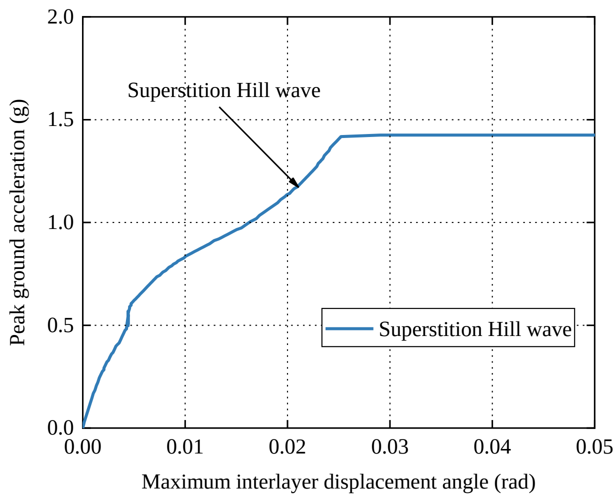

Fig. 7. IDA curve of unidirectional seismic waves

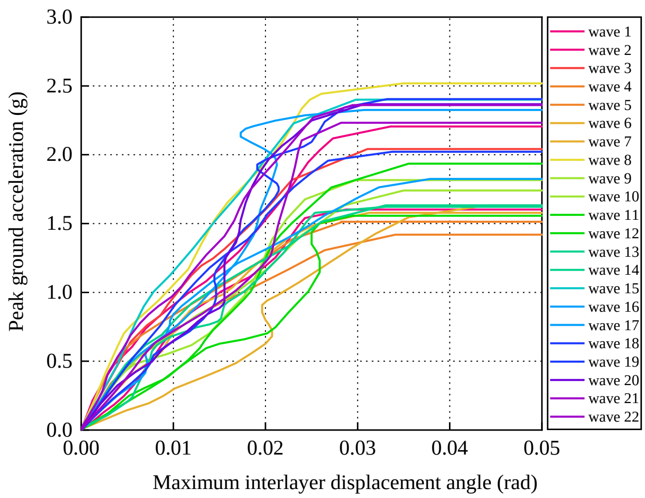

Fig.8. IDA curve of PGA and θ_{max}

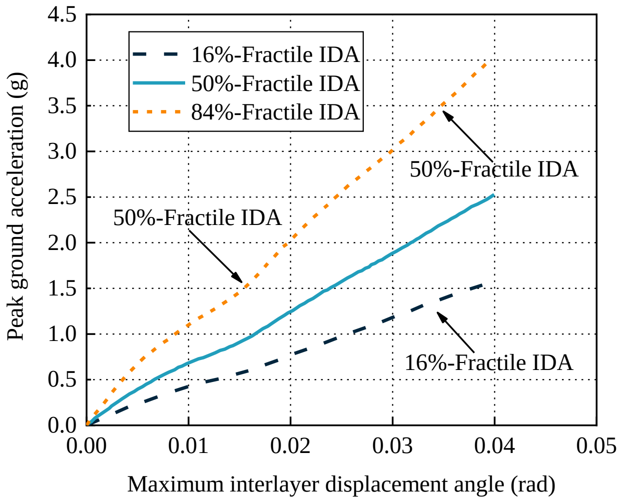

Fig. 9. Percentile curve

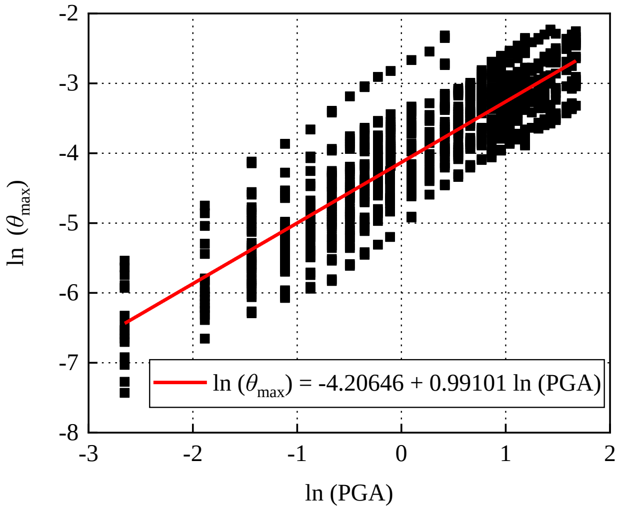

Fig. 10. Linear regression diagram of the turbine building

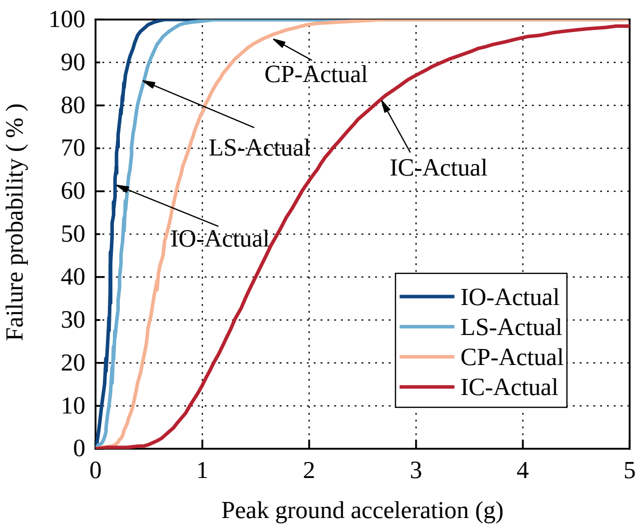

Fig. 11. seismic fragility curve of the turbine building

2) Seismic fragility assessment

In the case of relatively common and low-intensity Frequent earthquakes, the exceedance probabilities of the structure being in the Operational (OP) and Immediate Occupancy (IO) states are 14.4% and 2.3%, respectively. The exceedance probability reflects the likelihood of the structure surpassing the defined limits for each performance state under specific seismic actions. According to the FEMA guidelines, the reference exceedance probability is set at 50%. Since the exceedance probabilities for both states in this structure are lower than the value prescribed by FEMA, it indicates that the structure is capable of maintaining normal operation and being immediately usable during moderate earthquakes, with a relatively low risk of exceeding the corresponding performance state limits. This ensures the structural stability and safety in such conditions.

In the case of a Fortification earthquake, the exceedance probability for the structure being in the Life Safety (LS) state is only 0.71%. FEMA's prescribed exceedance probability for this state is 10%. Clearly, the exceedance probability of this structure is much lower than the prescribed value, indicating that the structure can effectively safeguard life safety during a design-level earthquake. The likelihood of a life-threatening situation occurring is extremely low, and the structure's performance can adequately withstand the impacts of the design-level earthquake, maintaining the overall stability of the structure and providing sufficient safety for the occupants.

For Rare earthquakes, known as extreme events, the exceedance probability for the structure being in the Collapse Prevention (CP) state is 0.18%. Comparing this with FEMA’s prescribed exceedance probability of 2% for this state, the structure’s exceedance probability is significantly lower. This strongly demonstrates that even under the extreme seismic impact of a rare earthquake, the structure still has a strong resistance to collapse, maintaining its overall stability to the greatest extent and minimizing the severe consequences of building collapse. This offers a critical defense line for the safety of both life and property.

IV. Parameter Analysis

In order to explore the influence of column reinforcement ratio and concrete strength on the vulnerability of structures and provide a basis for seismic design of turbine building, this paper conducts parameter analysis of column reinforcement ratio and concrete strength.

A. The influence of column reinforcement ratio on the fragility of turbine building

Under the condition that the structural reinforcement ratio checking calculation meets the requirements, the reinforcement ratio of the column is changed by changing the section size of the column. The above 22 seismic waves are used to analyze the seismic fragility of the turbine building based on the IDA method, and compared with the original cases to explore the influence of the reinforcement ratio of the column on the seismic fragility of the turbine building.

1) Case setting

Without changing the span, site category, seismic grouping, load, and other conditions of the original case, the section size of the column is modified to change the reinforcement ratio of the column, and the size of the A-axis column, B-axis column, and C-axis column is increased and decreased respectively. The section size of each case is shown in Table VII. Among them, Case One is the original case, Case Two and Case Three are the cases after changing the size of A shaft column, Case Four and Case Five are the cases after changing the size of B shaft column, Case Six and Case Seven are the cases after changing the size of C shaft column.

2) Seismic fragility curve

The obtained six cases are fitted by percentile curve. The percentile curve statistics of each case are shown in Fig. 12.

Log the results of IDA from condition 2 to condition 7. After the logarithm, the results were analyzed by the origin software. The probability demand function is established with the independent variable ln (PGA) and the dependent variable ln (θ_{max}).

The linear regression data are shown in Fig. 13. The unknown quantities a and b in the demand function of each case are obtained by linear regression curve analysis, as shown in Table VIII. The a and b values are brought into Eq. (3) to know the demand function of each case.

According to a, and b, the values of α and β can be obtained, as shown in Table IX.

Taking α and β into Eq. (5), the exceedance probability curves of each case are obtained. The seismic fragility curve can be obtained by bringing the PGA values of each case into its exceedance probability curve. The seismic fragility curves of each case under different limit states are shown in Fig. 14. The probability of each case exceeding the limit state is shown in Table X.

3) Seismic fragility assessment

The probability of preventing collapse of cases 2-7 is less than 2%, that is, the structure is considered to achieve the performance of no collapse under large earthquakes. Through the analysis of Fig. 14 and Table X, it can be seen that by changing the reinforcement ratio of the A-axis column, B-axis column, and C-axis column, it is concluded that the smaller the reinforcement ratio, the higher the structural fragility. When the number of column reinforcements is constant, increasing the column section will lead to a decrease in the reinforcement ratio of the column, increasing in the probability of exceeding the limit state, indicating that the seismic resistance of the structure is weakened. There are three specific reasons for the emergence of this result:

Columns with low reinforcement ratios, under seismic loading, cannot dissipate energy effectively through processes such as plastic deformation of reinforcement and concrete crushing, as is the case with columns with an appropriate reinforcement ratio, due to the premature yielding of the reinforcement and the brittle failure of the concrete. Columns with low reinforcement ratios have poor ductility and may experience sudden brittle failure under seismic loading. They do not have sufficient deformation capacity to accommodate ground motion and structural vibrations caused by the earthquake. As the reinforcement ratio decreases, columns are more likely to develop cracks and concrete damage during loading, leading to a rapid decrease in the column's stiffness. Under seismic loading, the reduction in stiffness causes changes in the structure's natural frequency, which further amplifies the structural vibration response, making the structure more vulnerable to damage and weakening its seismic performance.

TABLE V
LIMIT STATE POINTS OF THE IDA PERCENTILE CURVE

Percentile curve	Immediate Occupancy		Life Safety		Collapse Prevention		Incipient Collapse	
	θ_{max}	PGA / g	θ_{max}	PGA / g	θ_{max}	PGA / g	θ_{max}	PGA / g
16%	0.0025	0.12	0.004	0.18	0.01	0.42	0.025	0.97
50%	0.0025	0.20	0.004	0.30	0.01	0.68	0.025	1.57
84%	0.0025	0.33	0.004	0.53	0.01	1.10	0.025	2.54

TABLE VI
THE PROBABILITY OF EXCEEDING THE LIMIT STATE IN THE 8-DEGREE AREA

Earthquake effect	PGA / g	Immediate Occupancy	Life Safety	Collapse Prevention	Incipient Collapse
Frequent earthquake	0.07	14.40%	2.30%	0.00%	0.00%
Fortification earthquake	0.20	62.50%	26.70%	0.71%	0.00%
Rare earthquake	0.40	95.50%	77.60%	14.20%	0.18%

TABLE VII
COLUMN SECTION SIZE OF FRAME-BENT STRUCTURE OF DIFFERENT CASES

Cases	A-axis		B-axis		C-axis	
	Size / mm	Reinforcement ratio	Size / mm	Reinforcement ratio	Size / mm	Reinforcement ratio
One	2000×1100	1.20%	2000×1100	1.20%	1800×1100	1.80%
Two	2200×1100	1.10%	2000×1100	1.20%	1800×1100	1.80%
Three	1800×1100	1.30%	2000×1100	1.20%	1800×1100	1.80%
Four	2000×1100	1.20%	2200×1100	1.10%	1800×1100	1.80%
Five	2000×1100	1.20%	1800×1100	1.30%	1800×1100	1.80%
Six	2000×1100	1.20%	2000×1100	1.20%	2000×1100	1.60%
Seven	2000×1100	1.20%	2000×1100	1.20%	1600×1100	2.00%

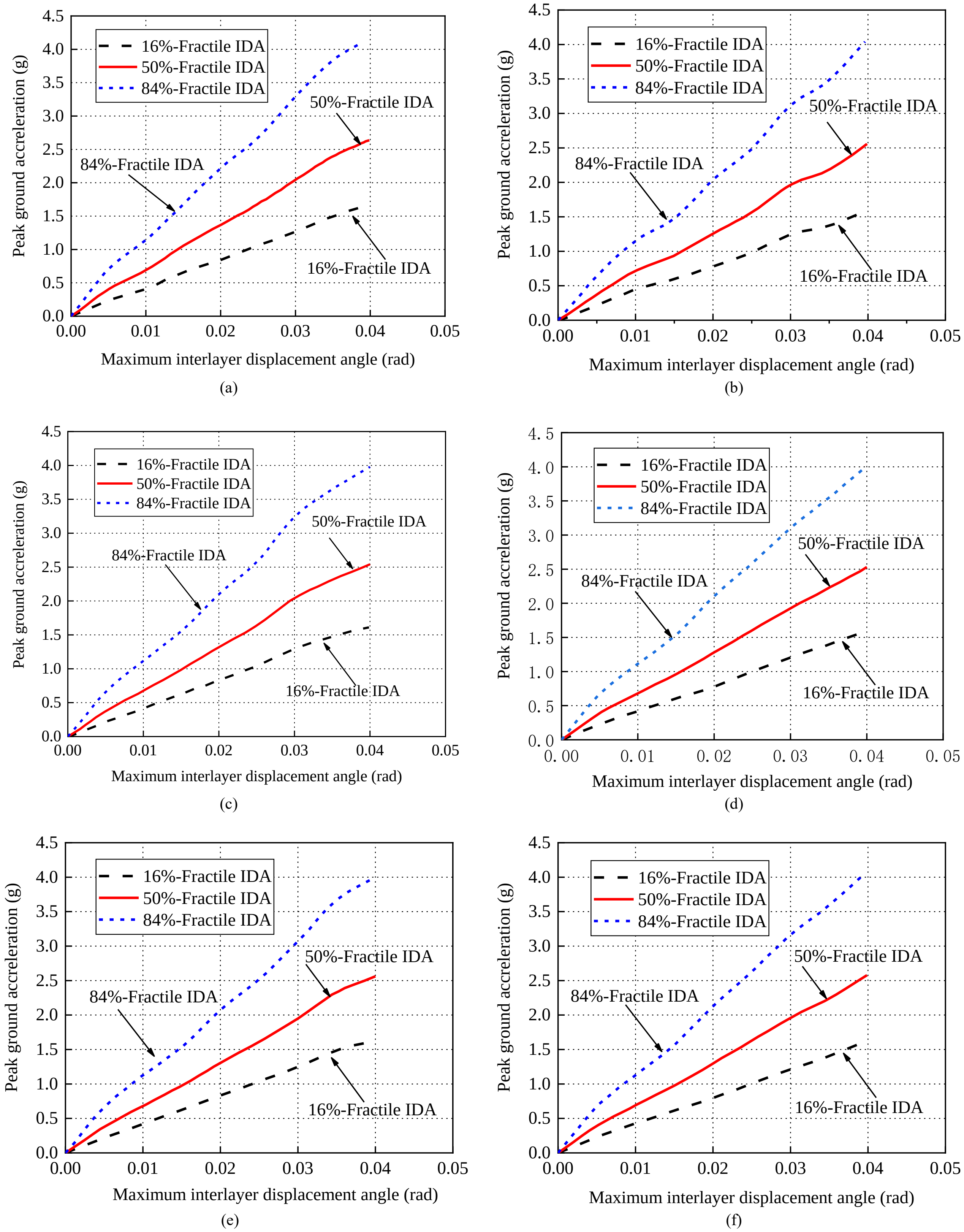

Fig. 12. Percentile curve of various cases: (a)The percentile curve of Case Two, (b)The percentile curve of Case Three, (c)The percentile curve of Case Four, (d)The percentile curve of Case Five, (e)The percentile curve of Case Six, (f)The percentile curve of Case Seven

TABLE VIII
VALUES OF A AND B OF DIFFERENT CASES

Cases	One	Two	Three	Four	Five	Six	Seven
a	*	-4.2416	-4.2674	-4.2223	-4.3145	-4.2206	-4.1992
b	0.9964	0.9733	0.9926	0.9644	1.0057	0.9866	1.0035

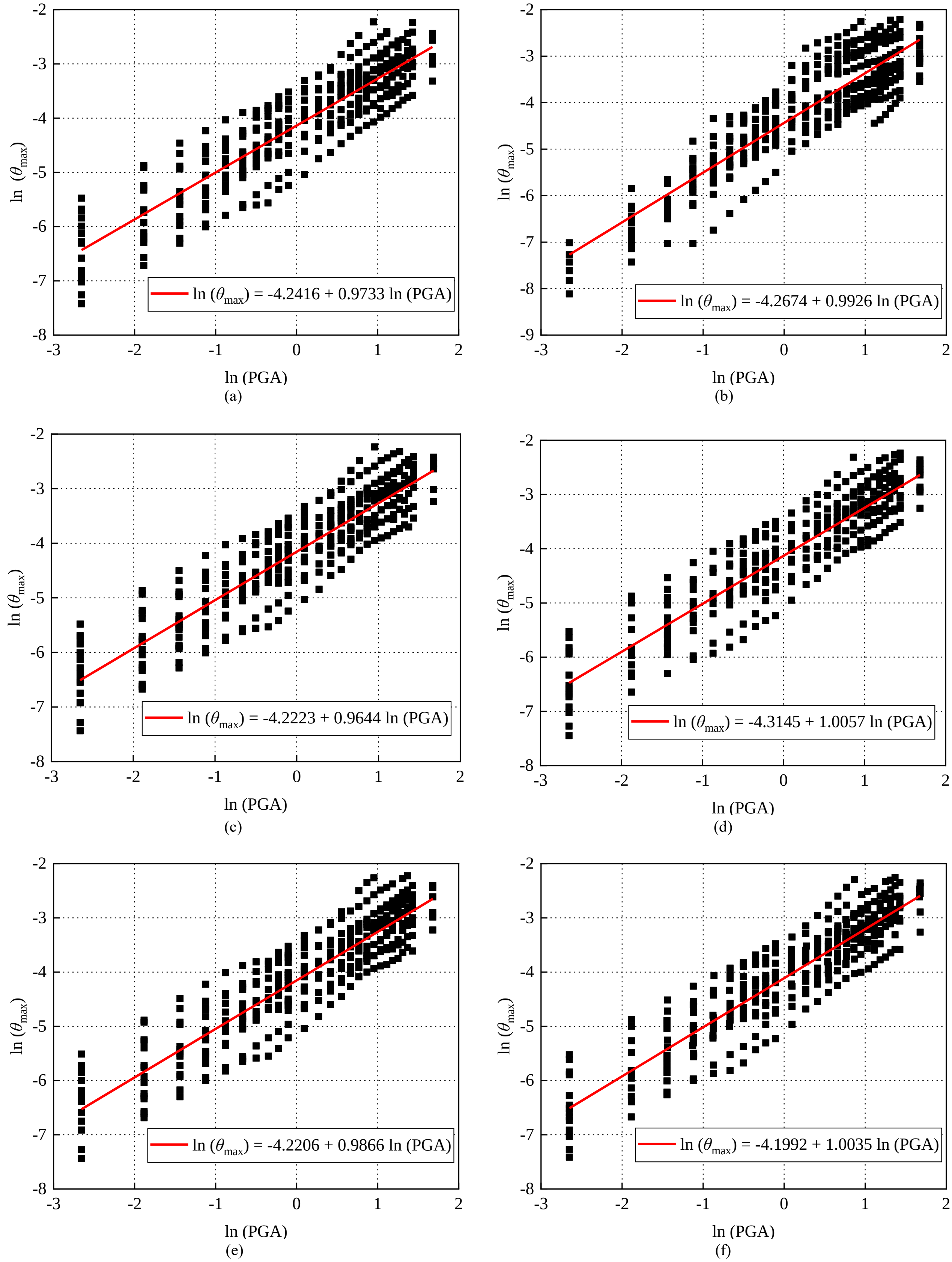

Fig. 13. Linear regression curve of different cases: (a) Linear regression curve of Case Two, (b) Linear regression curve of Case Three, (c) Linear regression curve of Case Four, (d) Linear regression curve of Case Five, (e) Linear regression curve of Case Six, (f) Linear regression curve of Case Seven

TABLE IX
REGRESSION CURVE PARAMETERS OF DIFFERENT CASE

Cases	One	Two	Three	Four	Five	Six	Seven
α	0.0146	0.0144	0.0140	0.0147	0.0134	0.0147	0.0150
β	0.9964	0.9733	0.9926	0.9644	1.0057	0.9866	1.0035

TABLE X
PROBABILITY OF EXCEEDING THE LIMIT STATE OF DIFFERENT CASE

Case	Earthquake effect	PGA / g	Immediate Occupancy	Life Safety	Collapse Prevention	Incipient Collapse
One	Frequent earthquake	0.07	14.40%	2.30%	0.00%	0.00%
	Fortification earthquake	0.20	62.50%	26.70%	0.71%	0.00%
	Rare earthquake	0.40	95.50%	77.60%	14.20%	0.18%
Two	Frequent earthquake	0.07	16.30%	2.70%	0.00%	0.00%
	Fortification earthquake	0.20	64.30%	28.30%	0.80%	0.00%
	Rare earthquake	0.40	95.00%	78.10%	14.50%	0.20%
Three	Frequent earthquake	0.07	13.10%	2.00%	0.00%	0.00%
	Fortification earthquake	0.20	60.00%	24.60%	0.50%	0.00%
	Rare earthquake	0.40	94.80%	75.50%	12.60%	0.15%
Four	Frequent earthquake	0.07	18.30%	3.20%	0.00%	0.00%
	Fortification earthquake	0.20	66.80%	30.60%	0.90%	0.00%
	Rare earthquake	0.40	96.20%	79.70%	15.80%	0.22%
Five	Frequent earthquake	0.07	10.10%	1.30%	0.00%	0.00%
	Fortification earthquake	0.20	54.60%	20.50%	0.40%	0.00%
	Rare earthquake	0.40	93.50%	71.60%	10.40%	0.09%
Six	Frequent earthquake	0.07	15.80%	2.60%	0.00%	0.00%
	Fortification earthquake	0.20	64.30%	28.30%	0.80%	0.00%
	Rare earthquake	0.40	95.90%	78.60%	14.90%	0.20%
Seven	Frequent earthquake	0.07	14.90%	2.40%	0.00%	0.00%
	Fortification earthquake	0.20	63.80%	27.9%	0.80%	0.00%
	Rare earthquake	0.40	96.00%	79.0%	15.20%	0.21%

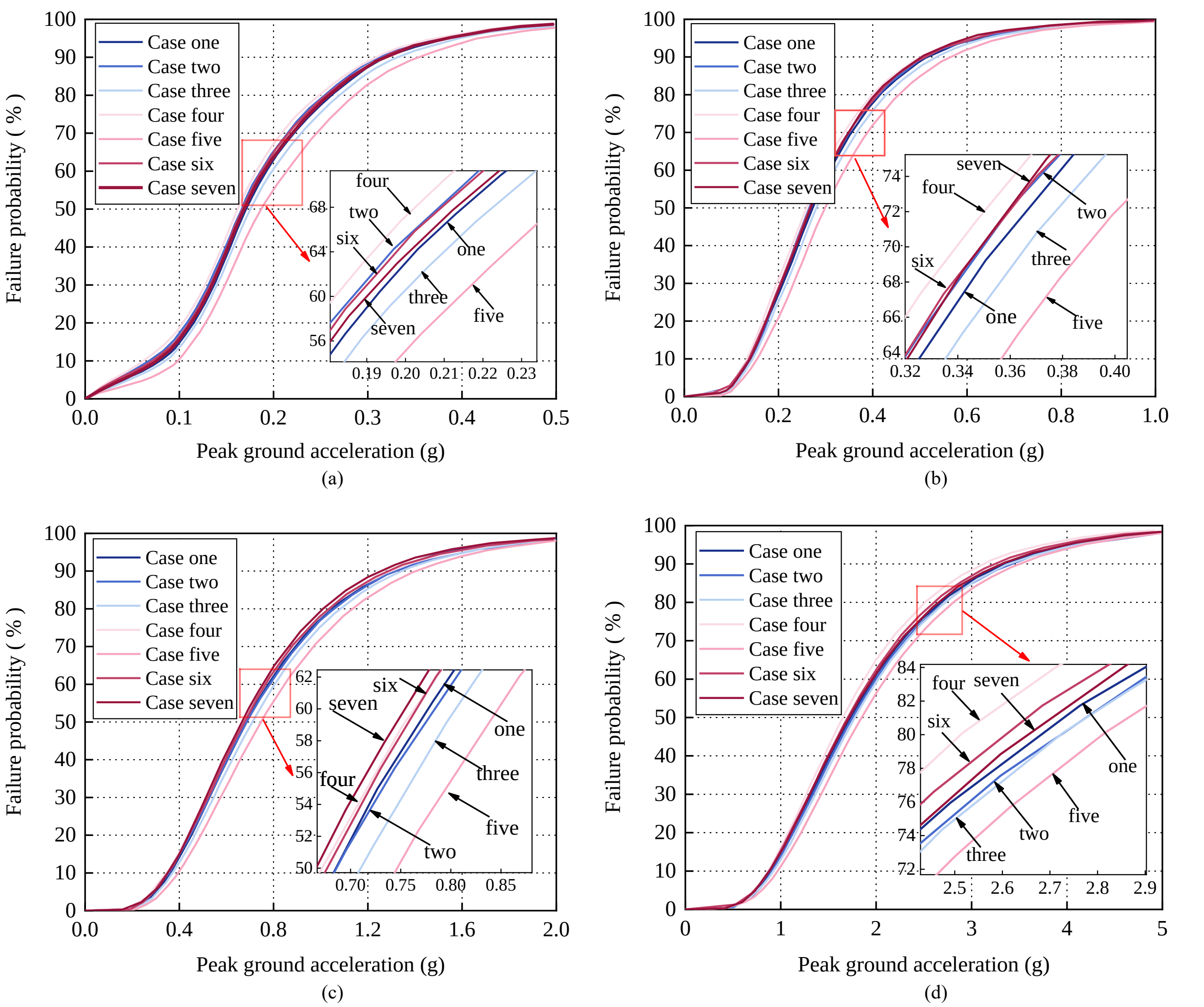

Fig.14. Seismic fragility curves of different cases under different states: (a) Seismic fragility curves under IO states, (b) Seismic fragility curves under LS states, (c) Seismic fragility curves under CP states, (d) Seismic fragility curves under IC states

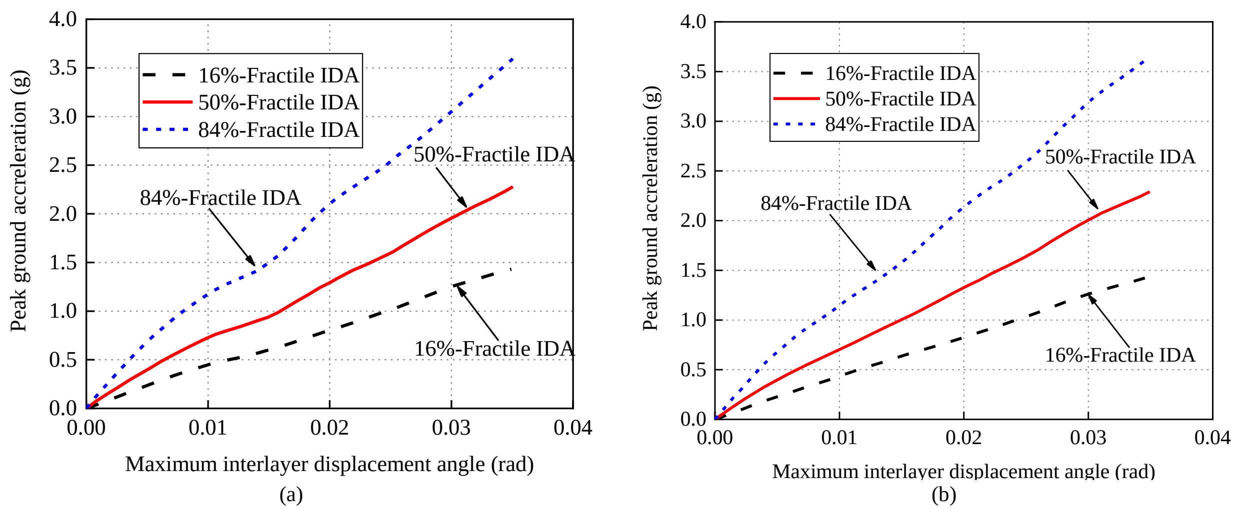

Fig. 15. Percentile curve of various case: (a)The percentile curve of Case Eight, (b)The percentile curve of Case Nine

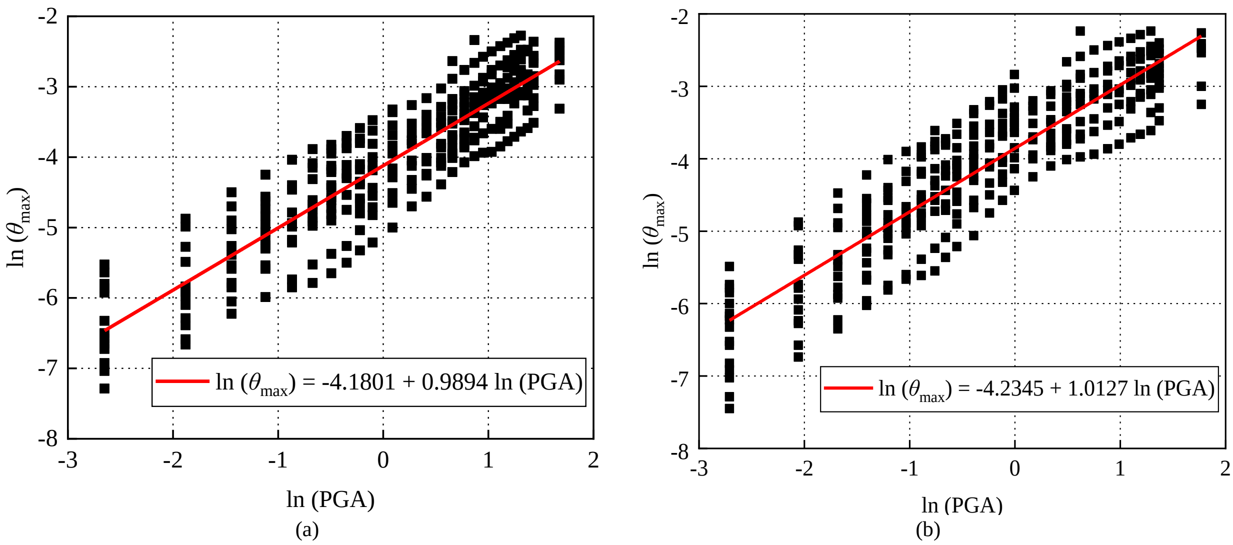

Fig. 16. Linear regression curve of different cases: (a) Linear regression curve of Case Eight, (b) Linear regression curve of Case Nine

B. The influence of concrete strength on the fragility of turbine building

1) Case setting

The influence of concrete strength on the seismic fragility of turbine building is explored by comparing Case Eight (C30), Case Nine (C50), and Case One (C40) with the same reinforcement ratio.

2) Seismic fragility curve

The percentile curve of Case Eight and Case Nine is fitted, and the statistical values of the percentile curve of each case are as follows Fig. 15 shows.

Log the results of IDA from condition eight and condition nine. After the logarithm, the results were analyzed by the origin software. The probability demand function is established with the independent variable ln (PGA) and the dependent variable ln (θ_{max}). The linear regression data are shown in Fig. 16. The unknown quantities a and b in the demand function of each case are obtained by linear regression curve analysis, as shown in Table XI. The a and b values are brought into Eq. (3) to know the demand function of each case.

According to a and b, the values of α and β can be obtained, as shown in Table XII. Taking α and β into Eq. (5), the exceedance probability curves of each case are obtained. The seismic fragility curve can be obtained by bringing the PGA values of each case into its exceedance probability curve. The seismic fragility curves of each case under different limit states are shown in Fig. 17. The probability of each case exceeding the limit state is shown in Table XIII.

3) Seismic fragility assessment

From Fig. 17 and Table XIII, it can be observed that there is a significant difference in the vulnerability between C30 and C40 concrete. Vulnerability is often associated with the likelihood of structural damage under various seismic or other disaster conditions, and the results are reflected through indicators such as failure probability. In this regard, C40 concrete has a clear advantage over C30 concrete. The use of C40 concrete can effectively reduce the failure probability, meaning that structures made with C40 concrete are less likely to experience damage under the same external loading, thereby enhancing the structural safety and reliability. The specific comparison of seismic performance of different types of concrete is as follows:

Normal Operating Condition (Frequent Earthquakes): Under frequent seismic events, which are relatively common and of lower intensity, C50 concrete reduces the failure probability by 2% compared to C40 concrete. This indicates that under frequent seismic conditions, C50 concrete slightly improves the structure's ability to maintain normal operation, reducing the likelihood of failure.

Collapse Prevention (Rare Earthquakes): In the case of rare, highly destructive seismic events, which aim to prevent structural collapse, C50 concrete only reduces the failure probability by 0.02% compared to C40 concrete. While there is a slight reduction, indicating that C50 concrete has slightly better seismic performance than C40 concrete, the numerical difference is very small. This suggests that under rare seismic conditions, even with C50 concrete, the improvement in seismic performance is not significant, and the ability of both concrete types to prevent collapse is quite similar.

TABLE XI
VALUES OF A AND B OF DIFFERENT CASES

Cases	One	Eight	Nine
a	/	-4.2416	-4.2674
b	0.9964	0.9733	0.9926

TABLE XII
REGRESSION CURVE PARAMETERS OF DIFFERENT CASES

Cases	One	Eight	Nine
α	0.0146	0.0153	0.0144
β	0.9964	0.9849	1.0127

TABLE XIII
PROBABILITY OF EXCEEDING THE LIMIT STATE OF DIFFERENT CASE

Case	Earthquake effect	PGA / g	Immediate Occupancy	Life Safety	Collapse Prevention	Incipient Collapse
One	Frequent earthquake	0.07	14.40%	2.30%	0.00%	0.00%
	Fortification earthquake	0.20	62.50%	26.70%	0.71%	0.00%
	Rare earthquake	0.40	95.50%	77.60%	14.20%	0.18%
Eight	Frequent earthquake	0.07	18.10%	3.20%	0.00%	0.00%
	Fortification earthquake	0.20	67.50%	31.30%	1.00%	0.00%
	Rare earthquake	0.40	96.50%	81.10%	17.10%	0.27%
Nine	Frequent earthquake	0.07	12.50%	1.80%	0.00%	0.00%
	Fortification earthquake	0.20	60.00%	23.60%	0.50%	0.00%
	Rare earthquake	0.40	95.10%	76.30%	13.20%	0.16%

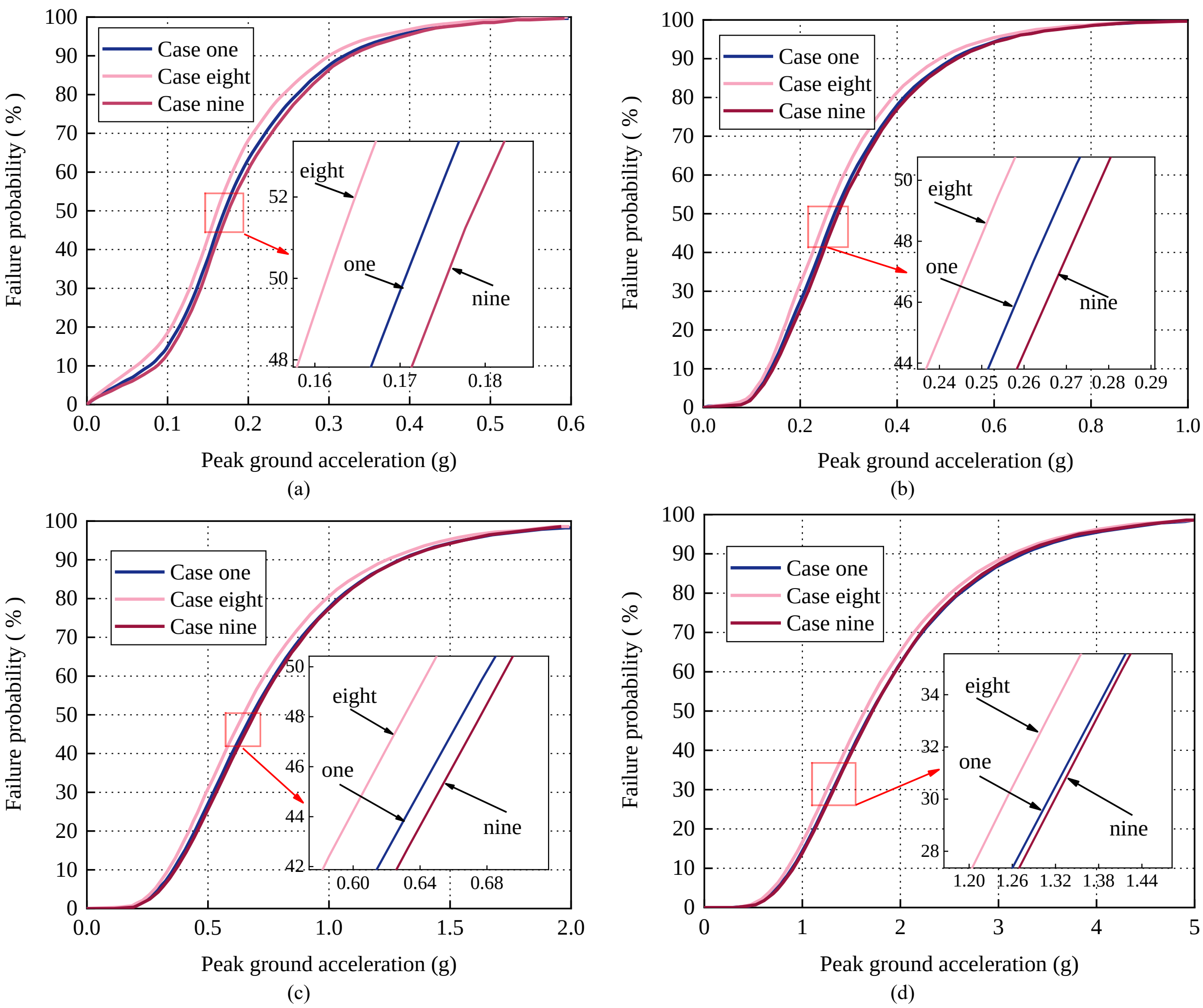

Fig. 17. Seismic fragility curves of different case under different states: (a) Seismic fragility curves under IO states, (b) Seismic fragility curves under LS states, (c) Seismic fragility curves under CP states, (d) Seismic fragility curves under IC states

V. Conclusion

This article establishes a turbine building model of NPP through the Open-source Software OpenSees, conducts seismic vulnerability analysis on the structure based on the IDA method, establishes a vulnerability curve to evaluate the seismic vulnerability of the turbine building structure, changes the reinforcement ratio and concrete strength to studies the influence of two types of parameters on the seismic performance of the model. The main conclusions are as follows:

1) The vulnerability curve shows that the designed and operated example turbine building in NPP can meet the seismic performance requirements in terms of exceedance probability under frequent earthquakes, fortification earthquakes, and rare earthquakes. The degree of damage in the turbine building is positively correlated with the seismic intensity parameters. Under the same seismic intensity parameters, the probability of slight, moderate, severe, and complete damage to the structure decreases in order.
2) Based on the structure of C40 concrete, the calculation of the structural fragility of different reinforcement ratios involves altering the reinforcement ratio of the A-axis column, B-axis column, and C-axis column. The research results indicate that the smaller the relative reinforcement ratio, the higher the structural failure probability. Increasing the cross-sectional area of the column without changing the amount of reinforcement will weaken the seismic performance of the structure. It is recommended to consider the total mass of concrete when designing the reinforcement ratio of the turbine building.
3) The seismic fragility of concrete with different strength grades vary under different seismic cases. C40 concrete shows a significant improvement in reducing failure probability compared to C30 concrete. However, while C50 concrete offers enhanced seismic performance compared to C40, the improvement is limited, especially under rare seismic events where the difference is minimal. This provides valuable reference for the selection of concrete materials in practical engineering, highlighting the need to consider multiple factors such as cost, construction difficulty, and the desired seismic performance when determining the appropriate concrete strength grade.

Overall, the performance state exceedance probabilities of the structure under multiple earthquake scenarios, including Frequent earthquakes, Fortification earthquakes, and Rare earthquakes, are all below the values specified by the FEMA guidelines. This clearly demonstrates that the structure possesses strong collapse resistance and, on top of meeting the required safety standards, offers a certain level of safety redundancy. This safety redundancy indicates that the structure has additional capacity to handle potential adverse factors that may exceed expectations, further enhancing its overall reliability and seismic performance. This provides strong support for the safe use of the structure throughout its entire lifespan.

References

[1] Wu J, Endo N, Saito M, "Cluster Analysis for Investigating Road Recovery in Fukushima Prefecture Following the 2011 Tohoku Earthquake," *Engineering Letters*, Vol. 29, no. 4, 2021.

[2] Li D, Endo N, "Daily Life Convenience of Post-disaster Recovery Housing Complexes Constructed in Fukushima Prefecture Following the 2011 Tohoku Earthquake," *Engineering Letters*, Vol. 32, no. 11, pp. 2173-2179, 2024.

[3] Cao Xu-Yang,Feng De-Cheng,and Li Yue, "Assessment of various seismic fragility analysis approaches for structures excited by non-stationary stochastic ground motions," *Mechanical Systems and Signal Processing*, Vol. 186, pp.109838-109859, 2023.

[4] Rajkumari S, Thakkar K, Goyal H, "Fragility analysis of structures subjected to seismic excitation: A state-of-the-art review," *Structures*, Vol. 40, pp. 303-316, 2022.

[5] Li F, Furong L, Guoxing C, "Nonlinear seismic responses of the soft rock site for nuclear power plants," *IOP Conference Series: Earth and Environmental Science*, Vol. 570, no. 2, pp.22-25, 2020.

[6] Pei Q, Wu C, Cheng Z, Ding Y, Guo H, "The Seismic Performance of New Self-Centering Beam-Column Joints of Conventional Island Main Buildings in Nuclear Power Plants," *Materials*, Vol.15, no. 5, pp. 1704-1731, 2022.

[7] Kwag S, Park J, Choi I-K, "Development of efficient complete-sampling-based seismic PSA method for nuclear power plant," *Reliability Engineering & System Safety*, Vol. 197, p. 106824, 2020.

[8] Zheng Z, Pan X, Bao X, "Seismic Fragility of a Typical Containment under Bidirectional Earthquake Excitations," *KSCE Journal of Civil Engineering*, Vol.22, no. 11, pp. 4430-4444, 2018.

[9] Ren L, Zhang G, Zhang Y, He S, "Seismic Fragility Analysis of V-Shaped Continuous Girder Bridges," *KSCE Journal of Civil Engineering*, Vol.24, no.3, pp.835-846, 2020.

[10] Ahmed K, Kim D, "A Windowed Adjustment Function Based NRC Compliant Ground Motions for Fragility Analysis of Base-Isolated Nuclear Power Plant," *KSCE Journal of Civil Engineering*, Vol. 22, no. 5, pp. 1900-1910, 2018.

[11] Ge F-W, Tong M-N, Zhao Y-G, "A structural demand model for seismic fragility analysis based on three-parameter lognormal distribution," *Soil Dynamics and Earthquake Engineering*, Vol. 147, p. 106770, 2021.

[12] Zhao C, Yu N, Mo YL, "Seismic fragility analysis of AP1000 SB considering fluid-structure interaction effects," *Structures*, Vol. 23, pp. 103-110, 2020.

[13] Zhao C, Yu N, Peng T, "Probabilistic seismic fragility assessment of isolated nuclear power plant structure using IDA and MSA methods. Structures," *Structures*, Vol. 34, pp. 1300-1311, 2021.

[14] Contiguglia CP, Pelle A, Briseghella B, Nuti C, "IMPA versus Cloud Analysis and IDA: Different Methods to Evaluate Structural Seismic Fragility," *Applied Sciences*, Vol. 12, pp.3687-3707, 2022.

[15] Pei Q, Qi P, Ma F, Cui D, Xue Z, Ding Y, "Resistance of Gable Structure of Nuclear Island to Progressive Collapse in Conventional Island Shield Building of Nuclear Power Plants," *Buildings*, Vol. 13, no. 5, pp1257-1283, 2023.

[16] Cheng F, Li J, Zhou L, Lin G, "Fragility analysis of nuclear power plant structure under real and spectrum-compatible seismic waves considering soil-structure interaction effect," *Engineering Structures*, Vol.280, p.115684, 2023.

[17] Zhao C, Yu N, Oz Y, Wang J, Mo YL, "Seismic fragility analysis of nuclear power plant structure under far-field ground motions," *Engineering Structures*, Vol. 219, p. 110890, 2020.

[18] De Borbón F, Domizio M, Ambrosini D, Curadelli O, "Influence of various parameters in the seismic soil-structure interaction response of a nuclear power plant," *Engineering Structures*, Vol.217, p. 110820, 2020.

[19] Nguyen D-D, Thusa B, Park H, Azad MS, Lee T-H, "Efficiency of various structural modeling schemes on evaluating seismic performance and fragility of APR1400 containment building," *Nuclear Engineering and Technology*, Vol. 53, no. 8, pp. 2696-2707, 2021.

[20] Kim C, Cha EJ, Shin M, "Seismic performance assessment of NPP concrete containments considering recent ground motions in South Korea," *Nuclear Engineering and Technology*, Vol. 54, no. 1, pp. 386-400, 2022.

[21] Pei Q, Cai B, Zhang L, Xue Z, Qi P, Cui D, Xueting Wang, "The Progressive Collapse Resistance Mechanism of Conventional Island Shield Buildings in Nuclear Power Plants," *Buildings*, Vol. 13, no. 4, pp. 958-984, 2023.

[22] Jha S, Roshan AD, Pisharady AS, Bishnoi LR, “Seismic Margin Assessment for earthquake beyond design basis – Simplified practical approach,” *Nuclear Engineering and Design*, Vol. 323, no. 1, pp. 329-337, 2017.

[23] Xu Z-H, Bai G-L, Zhao J-Q, “Experimental and numerical investigation on seismic performance of SRC variable-column exterior joints in CAP1400 NPP,” *Structures*, Vol.29, pp. 663-683, 2021.

[24] Qiang Pei, Yingzhu Zhong, Bo Wang, Pengfei Qi, Zhicheng Xue, Di Cui, Yu Ding, Bangwen Cai, “Performance of SRC unequal-depth beam-column irregular joint in NPP under progressive collapse,” Structures, Vol. 70, p.107593, 2024.

[25] Xu Z-H, Zhao J-Q, Bai G-L, Ding Y-G, “Incremental dynamic analysis of SRC frame-bent structures in CAP1400 NPP,” Nuclear Engineering and Design, Vol. 426, p. 113360, 2024.

[26] Sheng G, Jin S, Ma L, Bai Q, Xu C, Wang X, “A Quantitative Method for Seismic Robustness of RC Frame Considering Resistance Vulnerability of Column and Storey Drift Ratios,” KSCE Journal of Civil Engineering, Vol. 28, no. 1, pp. 231-249, 2024.

[27] Feng D-C, Cao X-Y, Wang D, Wu G, “A PDEM-based non-parametric seismic fragility assessment method for RC structures under non-stationary ground motions,” *Journal of Building Engineering*, Vol. 63, p. 105465, 2023.

[28] Dabaghi M, Saad G, Allhassania N, “Seismic Collapse Fragility Analysis of Reinforced Concrete Shear Wall Buildings,” *Earthquake Spectra*, Vol. 35, no.1, pp. 383-404, 2019.

[29] Ma W, “Incremental dynamic analysis method application in the seismic vulnerability of infilled wall frame structures,” *Journal of Vibroengineering*, Vol.27, no. 1, pp. 343-358, 2024.

[30] Nazari YR, Saatcioglu M, “Seismic vulnerability assessment of concrete shear wall buildings through fragility analysis,” *Journal of Building Engineering*, Vol. 12, pp. 202-209, 2017

[31] Ratnasari V, Utama SH, Dani ATR, “Toward Sustainable Development Goals (SDGs) with Statistical Modeling: Recursive Bivariate Binary Probit,” *IAENG International Journal of Applied Mathematics*, Vol. 54, no.8, pp. 1515-1521, 2024.

[32] Yu X-H, Dai K-Y, Li Y-S, “Variability in corrosion damage models and its effect on seismic collapse fragility of aging reinforced concrete frames,” *Construction and Building Materials*, Vol. 295, p.123654, 2021.

[33] Xu C, Deng J, Peng S, Li C, “Seismic fragility analysis of steel reinforced concrete frame structures based on different engineering demand parameters,” *Journal of Building Engineering*, Vol. 20, pp. 736-749, 2018.

[34] Adhitya BB, Costa A, Verawati K, “Study on the Failure Performance of Reinforced Concrete and Composite Concrete Structures due to Non-Linear Time History Earthquake Loads,” *Engineering Letters*, Vol. 31, no. 2, pp. 544-553, 2023.

[35] Zhao Y-G, Qin M-J, Lu Z-H, Zhang L-W, “Seismic fragility analysis of nuclear power plants considering structural parameter uncertainty,” *Reliability Engineering & System Safety*, Vol. 216, p.107970, 2021.

[36] Iervolino I, “Estimation uncertainty for some common seismic fragility curve fitting methods. Soil Dynamics and Earthquake Engineering,” *Soil Dynamics & Earthquake Engineering*, Vol. 152, p. 107068, 2022.

[37] Chang S, Jeon B, Kwag S, Hahm D, Eem S, “Seismic Performance of Piping Systems of Isolated Nuclear Power Plants Determined by Numerical Considerations,” *Energies*, Vol. 14, no. 13, pp.4028-4044, 2021.

[38] Yoon S, Lee DH, Jung H-J, “Seismic fragility analysis of a buried pipeline structure considering uncertainty of soil parameters,” *International Journal of Pressure Vessels and Piping*, Vol. 175, p.103932, 2019.

[39] Lu ELG, Garciano LEO, Flores FKS, Peradilla MS, Ong CY, Azcarraga AP, “Integrity Monitoring of Vertical and Horizontal Structures via Visualization and Statistical Inspection of a Mesh Sensor Network,” Vol. 30, no. 2, pp. 420-437, 2022.

[40] Biglari M, Ikeda Y, Kawase H, “Fragility curves of sequential earthquakes for RC buildings in Japan,” *Bulletin of Earthquake Engineering*, Vol. 22, no.9, pp. 4657-4676, 2024.

[41] Nguyen D-D, Thusa B, Han T-S, Lee T-H, “Identifying significant earthquake intensity measures for evaluating seismic damage and fragility of nuclear power plant structures,” *Nuclear Engineering and Technology*, Vol. 52, no. 1, pp. 192-205, 2020.

[42] Gorji Azandariani M, Gholami M, “Seismic fragility investigation of hybrid structures BRBF with eccentric-configuration and self-centering frame,” *Journal of Constructional Steel Research*, Vol. 196, p. 107300, 2022.

[43] Kumar M, Whittaker AS, “Effect of seismic hazard definition on isolation-system displacements in nuclear power plants,” *Engineering Structures*, Vol. 148, pp. 424-435, 2017.

[44] Kazantzi AK, Karaferis ND, Melissianos VE, Bakalis K, Vamvatsikos D, “Seismic fragility assessment of building-type structures in oil refineries,” *Bulletin of Earthquake Engineering*, Vol. 20, no. 12, pp. 6853-6876, 2022.

[45] Wang L, Geng P, Chen J, Wang T, “Machine learning-based fragility analysis of tunnel structure under different impulsive seismic actions,” *Tunnelling and Underground Space Technology*, Vol. 133, p. 104953, 2023.

[46] Guillermo Aldama-Bustos,Iain J. Tromans, Fleur Strasser, Graham Garrard, Guy Green, Liz Rivers, John Douglas, Roger M. W. Musson, Simon Hunt, Angeliki Lessi-Cheimariou, Manuela Daví, Colin Robertson, “A streamlined approach for the seismic hazard assessment of a new nuclear power plant in the UK,” *Bulletin of Earthquake Engineering*, Vol. 17, no. 1, pp. 37-54, 2019.

[47] Rohmer J, Gehl P, Marcilhac-Fradin M, Guigueno Y, Rahni N, Clément J, “Non-stationary extreme value analysis applied to seismic fragility assessment for nuclear safety analysis,” *Natural Hazards and Earth System Sciences*, Vol. 20, no. 5, pp. 1267-1285, 2020.

[48] Guo Q, Wang W, Xiong Y, Shi Y, “Cross-correlation Analysis Method on Explosion Seismic Waves Data,” *Engineering Letters*, Vol. 28, no. 4, pp. 1145-1151, 2020.

[49] Ruggieri S, Calò M, Cardellicchio A, Uva G, “Analytical-mechanical based framework for seismic overall fragility analysis of existing RC buildings in town compartments,” *Bulletin of Earthquake Engineering*, Vol. 20, no. 15, pp. 8179-8216, 2022.

[50] Guo Q, Wang W, Xiong Y, Zheng S, “Data Pre-processing Method of Explosion Seismic Waves Based on Cross-Correlation Analysis,” *Engineering Letters*, Vol. 31, no. 4, pp. 1656-1666, 2023.

[51] Elbostani S, El Jid R, “A Meshless Method Based on the Moving Least Squares Approach for Approximate Solution of the Generalized 2-D Nonlinear Benjamin–Bona–Mahony–Burgers Equation,” *IAENG International Journal of Applied Mathematics*, Vol. 54, no. 9, pp. 1734-1746, 2024.

[52] Dani ATR, Fauziyah M, Budiantara IN, “Statistical Modeling: A New Regression Curve Approximation using Mixed Estimators Truncated Spline and Epanechnikov Kernel,” *Engineering Letters*, Vol. 31, no. 4, pp. 1649-1655, 2023.

[53] Gentile R, Galasso C, “Gaussian process regression for seismic fragility assessment of building portfolios,” *Structural Safety*, Vol. 87, p. 101980, 2020.